Applied Catalysis B: Environmental 227 (2018) 433–445

Contents lists available at ScienceDirect

Applied Catalysis B: Environmental

journal homepage: www.elsevier.com/locate/apcatb

Controlled Synthesis of highly proficient and durable hollow hierarchical heterostructured (Ag-AgBr/HHST): A UV and Visible light active photocatalyst in degradation of organic pollutants

Muhammad Shakeel[a], Baoshan Li[a,*], Muhammad Arif[a], Ghulam Yasin[a,b], Wajid Rehman[c,d], Arif Ullah Khan[a], Shafiullah Khan[e], Abrar Khan[a], Jawad Ali[a]

[a] State Key Laboratory of Chemical Resource Engineering, Beijing University of Chemical Technology, Beijing, 100029, PR China
[b] College of Energy, Beijing University of Chemical Technology, Beijing, 100029, PR China
[c] Technical Institute of Physics and Chemistry, Chinese Academy of Sciences, Beijing, 10090, PR China
[d] Department of Chemistry, HAZARA University, Mansehra, 21120, KPK, Pakistan
[e] Institute of Chemical Sciences, Gomal University, D.I.Khan, KPK, Pakistan

ARTICLE INFO

Keywords:
Ag-AgBr/HHST
Heterostructure
Effect of calcination
UV and visible light responsive
Photocatalytic performance

ABSTRACT

Progression in nano technology enormously influence on the synthesis of highly proficient photo materials and investigate their applications in diverse fields. A novel mesoporous heterostructure Ag-AgBr/HHST (hollow hierarchical silica-titania supported silver-silverbromide), synthesized by a facile one-pot micro emulsification method at controlled calcination temperature and investigated its photocatalytic performance for the degradation of methyl orange and aniline as ultra violet and visible light responsive material. Mesoporous Ag-AgBr/HHST was characterized by X-ray diffraction (XRD), scanning electron microscopy (SEM), high-resolution transmission electron microscopy (HRTEM), UV–vis. diffuse reflectance spectroscopy (UV–vis. DRS), Nitrogen adsorption-desorption analysis, photoelectron spectroscopic measurements (XPS) and photoluminescence spectral analysis (PL). The XRD, HRTEM and optical spectroscopic analysis justified the incredible effect of calcination temperature on the structure and morphology of nano composite. The results indicates, the photocatalyst synthesized at optimum calcinations temperature (550 °C) consist of small-hollow-spheres@big-hollow-spheres, leading the Ag and AgBr nano particles with an average particle size of 2–8 nm are homogeneously distributed on the surface of the hollow hierarchical silica-titania matrix, some particles are deeply embedded in HHST. Due to exceptional morphology, high surface area, small particles size and porous structure, the Ag-AgBr/HHST revealed elevated photocatalytic performance to degraded the 200 mL (200 ppm) of each methyl orange and aniline under simulated ultra violet as well as visible light irradiations in very short time intervals. Hollow hierarchical silica-titania offer high-quality conducting channel to pick up mass loading and enhance charge transfer. Whereas, strong connection of Ag and AgBr with silica-titania, feature highly active sites that causes synergetic effect capable for commendable photocatalytic performance compared with individual HHST, Ag-AgBr and (Degussa P25). While the photocatalyst obtained at 650 °C have some extant of phase conversion starting anatase to rutile phase of titania, and consist of big sized aggregated nano particles. The recycling runs experiments and reusability of the photocatalyst illustrate the venerable stability of the material that strengthens the synthesis of novel hollow hierarchical mesoporous compounds in this domains.

1. Introduction

Environmental problems are massively increasing with the passage of time, usually the discharge of industrial effluents into the aqueous environment can directly impact on living environment and frustrate society advancement. Generally, dyes used in textiles and paper industries are considered well known organic contaminants. It is very painful to degrade them entirely by any common conventional physical, chemical or biological technique, yet on account of their structural stability and resistance to biodegradation [1,2]. Therefore, to build up a highly efficient, clean and cost-effective technology for decaying health hazardous organic contaminants has always been the pursuit of environmental remediation [3,4]. Nano photo-technology is the most promising, low-cost and effective technique, introducing a range of

* Corresponding author.
E-mail address: bsli@mail.buct.edu.cn (B. Li).

https://doi.org/10.1016/j.apcatb.2018.01.037
Received 10 August 2017; Received in revised form 14 December 2017; Accepted 16 January 2018
Available online 31 January 2018
0926-3373/

nano structure systems applied for photocatalytic degradation of lethal organic contaminants into carbonaceous products [5–7]. In this regards TiO_2 has been recognized as a vital material, due to its photochemical stability, non-toxicity, low cost, high competency for photochemical energy conversion [8,9]. However TiO_2 could be sensible only in the UV light region that accounts less than 5% of the sunlight [10]. The efficient utilization of sunlight, required to reallocate the absorption band of semiconductor from UV to visible light region, either by doping with metal and connecting with other semiconductors to figured heterostructure or influencing its bulk and surface physicochemical properties, such as crystal structure, crystalline nature, and adsorption capability can also enhance its photocatalytic activities [11–16]. In fastidious, the fabrication of mesoporous hollow hierarchical heterostructure photocatalyst has rewarded extra consideration, due to its large surface areas, ordered porous structures and large pore volumes that enlarge the surface reactive sites and improved mass transportation. The previous studies focus point is the photosensitization of TiO_2 based semiconductors either under UV light or visible light irradiations and investigated their photocatalytic performance but these materials not satisfied the needful requirements due to many flaws to utilize the maximum spectrum of solar light, shortcomings also includes very long photo degradation time intervals and practical instability of the materials, hence economically misfit their use for further applications [17–20]. In our former studies we have prepared foamed silica-titania nano composite, but it is also purposeful only under the illumination of ultra violet light to degrade the methyl orange [21]. The plan of this work is to move the absorption band of light toward visible region by utilizing maximum spectrum of solar light and also boost the stability and photocatalytic effectiveness of silica-titania based nano composite both as an ultra violet and visible light approachable material that has the ability to degrade the stable organic compounds in very short time intervals. This has been done by doping with Ag and AgBr and controlling its hollow hierarchical morphology at optimum calcination temperature (550 °C). Loading of Ag and AgBr on the surface of silica-titania to becomes a sentimental visible light responsive photocatalyst, because in all noble metals silver and silver bromide has taken keen interest, due to the extraordinary photo-sensitivities of AgBr in visible light region and owing to the stable surface plasmon resonance(SPR) effect of Ag nano particles, The Ag nano particles boost the band gap separation and reduce electrons-hole recombination that can drastically increase the stability of nano composite hence enhance the photocatalytic performance [22,23].

Herein we report a novel compound with hollow hierarchical mesoporous silica-titania decorated by Ag and AgBr NPs that synthesized via micro-emulsification method as specified in schematic illustrations (Fig. S7). This novel material acquired large surface area and unusual hollow porous structure, which can readily afford active sites for the gathering of Ag and AgBr nano particles. Furthermore, both the size and distribution of Ag and AgBr nano particles and hollow morphology of the nano composite can be facilely controlled via properly tuning the calcination temperature (150 °C, 250 °C,350 °C, 450 °C, 550 °C and 650 °C).

Whereas the samples obtained at optimum calcination temperature (550 °C) was investigated for photo-catalytic degradation of methyl orange (MO) and aniline under the influence of simulated ultra violet as well as visible light. The results demonstrated that Ag-AgBr/HHST comprise superior photocatalytic capability as compared to individual HHST, Ag-AgBr and (Degussa P25), consequently considered as pre-eminent innovation in the field of environmental pollution remediation.

2. Experimental section

2.1. Materials

Aqueous ammonia solution (25 wt%), Tetraethyl orthosilicate (TEOS, A.R) and Ethanol (A.R) were purchased by Xilong Chemical Company China. n-octane (A.R), Cetyltrimethyl ammonium bromide (CTAB, A.R), and Methyl Orange (A.R) and Aniline (A.R) were purchased from Tianjin Fuchen Chemical Reagents Industry China. Tetra-Butyl Ortho-Titanate (TBOT, A.R), Methanol (A.R) and Silver Nitrate ($AgNO_3$, A.R), were purchased from Beijing Chemicals Reagent Co., Ltd. All the materials were of analytical grade and used throughout the study without further purification.

2.2. Synthesis of the photocatalyst

Silver-silver bromide supported hollow hierarchical silica-titania mesoporous nano composite (Ag-AgBr/HHTS) was prepared by a facile one-pot micro emulsification method.

First of all the silica-titania precursor was prepared by dissolving 2.3 g of tetrabutyl ortho titanate into a blend of acetyl-acetone and n-octane (1:1.5) by volume. The resultant mixture stirred for 30 min at room temperature to acquire a yellow solution. Then 6.8 mL of TEOS was added into the dispersion with constant stirring for another 30 min to get hold of silica-titania precursor. On other hand, the foaming reagent was prepared by dissolving 1.40 g of CTAB in a mixture of 70 mL deionized water and 20 mL octane to form micro emulsion, then added 15 mL of aqueous ammonia (2 $molL^{-1}$) with stirring. Afterward the silica-titania precursor was added drop wise into the freshly prepared micro emulsion for foaming with energetic stirring at room temperature till the completion of the reaction, that result in the formation of hollow hierarchical silica-titania support. At the end, 18 mL (0.2 M) stable silver-ammonia solution was added to the resulting mixture and stirred for 1 h. During the reaction Ag^+ from $AgNO_3$ and Br^- from CTAB react to form AgBr, and deposited on the surface of hollow hierarchical silica-titania. Subsequently the mixture was autoclaved in a Teflon-lined stainless steel vessel at 373 K for 24 h. Later on the pellets of the mixture was separated by centrifugation at 3000 rmp, washed several times with deionized water and ethanol, and air dried at 333 K for 24 h. Finally this was calcined at different temperatures (150 °C, 250 °C, 350 °C, 450 °C, 550 °C and 650 °C) for 4 h, for each set of reaction to get the AgBr/HHST nano composite. After calcination AgBr/HHST was dispersed in de-ionized water with vigorous stirring and radiate under UV light for 60 min which accelerate the photolysis of AgBr to reduce partially Ag^+ to Ag NPs. The product was centrifuged and thoroughly rinsed with de-ionized water and dried at 333 K. The prepared as-sample is designated Ag-AgBr/HHST(T-1), Ag-AgBr/HHST(T-2), Ag-AgBr/HHST(T-3), Ag-AgBr/HHST(T-4) and Ag-AgBr/HHST(T-5), Ag-AgBr/HHST(T-6) obtained at different calcination temperatures respectively.

2.3. Characterization of the material

The crystalline structure of the products obtained at different calcination temperatures was characterized using X-ray diffraction, a Rigaku D/Max 2500 VBZ + /PC diffraction meter using Cu-Ka radiation (k = 0.1541 nm). The data for examination was collected in the 2θ range of 10 − 70°.The morphology and microstructure was studied by scanning electron microscope (SEM) Hitachi S-4700 and high-resolution transmission electron microscopy (HRTEM) JEM-3010 with an accelerating voltage of 200 kV measurements respectively. The elemental analysis and mapping was investigated by an energy dispersive spectroscopy (EDS). The nitrogen adsorption-desorption isotherms was obtained for surface area and pore size distribution by using a Micromeritics ASAP2020 M instrument. The materials was degassed in vacuum at 573 K for 6 h prior to measurements. The specific surface area was calculated by Brunauer-Emmett-Teller (BET) equation and the pore size distribution was calculated by Barrett-Joyner-Halenda (BJH) technique. UV–vis./NIR Spectrophotometer cary 500 scan with an integrating sphere attachment, UV–3600 (Shimadzu) used to record the UV–vis. diffuse reflectance spectra. The X-rays photoelectron spectroscopy (XPS) was carried out on ESCALAB-250. X-ray photoelectron

spectrometer with a monochromated Al-Kα X-ray (150 W), under the energy for survey is 200 eV while 30 eV for high resolution scan. The calibration of binding energy was carried out by setting C1 s peak to 284.6 eV. The photoluminescence (PL) spectra were recorded by Hitachi analytical instrument Model F-7000, Fluorescence Spectrophotometer with an excitation wavelength at 360 nm. The charging current density and electrochemical impedance spectroscopic (EIS) analysis was carried out to investigate the charge transfer and recombination rate during the photocatalytic reaction, the results was recorded on (CHI660E CH. Instrument Co. USA), electrochemistry work station in 1 M KOH solution at ambient temperature. The measurements was carried out in a three-electrode electrochemical cell with Pt wire used as counter and Ag/AgCl (PINE, 4 M KCl) as reference electrodes, while the Ni-foam with diameter of 1 cm^2 used as working electrode. Electron paramagnetic resonance (EPR) spectra was recorded at ambient temperature on an analytical instrument Bruker model E-500 spectrometer setting with modulation frequency was 100 KHz, modulation amplitude was 2.0 G, sweep width was 100.0 G, time constant 40.96 ms conversion 40.0 ms sweep time 80.72 s receiver gain was 5.02×10^3. The microwave power was 10.03 mW, and the frequency was 9.86 GHz and DMPO (Sigma Chemical Co.) was used as spin-trapping reagent.

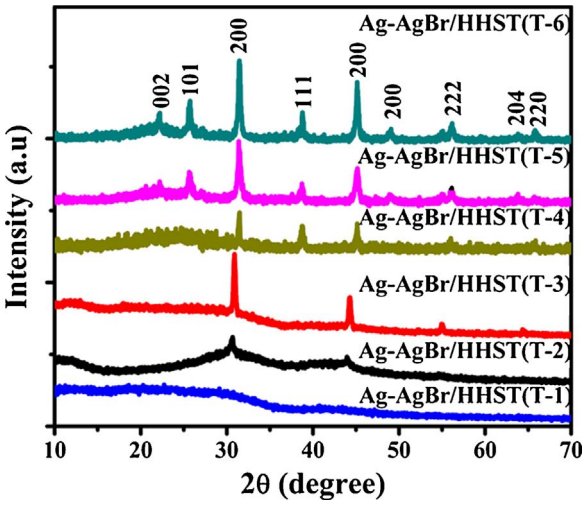

Fig 1. XRD patterns of different samples treated at different calcination temperatures Ag-AgBr/HHST(T-1) at 150 °C, Ag-AgBr/HHST(T-2) at 250 °C, Ag-AgBr/HHST(T-3) at 350 °C, Ag-AgBr/HHST(T-4) at 450 °C, Ag-AgBr/HHST(T-5) at 550 °C and Ag-AgBr/HHST(T-6) at 650 °C.

2.4. Measurement of photo catalytic performance

To evaluate the photocatalytic activity of the as-prepared samples, we prefer methyl orange and aniline as noxious S and N containing organic pollutants. In a usual trial 0.2 g of the samples was dispersed in a 200 mL(200 ppm) aqueous solution of each pollutant, followed by added in pyrex reactor, the suspension was sonicated in dark for 30 min to establish well the adsorption-desorption equilibrium between pollutants and the photocatalyst prior to light irradiations. A tungsten lamp with cut-off filter paper used as visible-light source and xenon lamp as UV light source for photocatalytic degradation reaction. After that the reactor was exposed to the ultra violet and visible light in two different experiments with steady stirring. After definite irradiations time intervals, the suitable amount of sample pipette out from the reaction system and centrifuge it at 3000 rpm. Then pallets of photocatalyst settle down and the supernatant was examined for the degradation of organic pollutants by using UV–vis. spectrophotometer, the methyl orange at 468 nm and aniline was examined at 265 nm. The change in concentration of each dye was calculated from their respective absorption peaks comparing with the standard calibration curve. Finally degraded quantity of the each pollutants at particular irradiation time intervals was calculated by plotting C/Co vs time. The Co is the initial concentration and C is the equilibrium concentration at reaction time t.

The stability of the photocatalyst was investigated by using cycling runs experiments. After the irradiations for specific time intervals, the suspension was filtered and the photocatalyst was washed severally with absolute alcohol and water, dried at 373 K for 8 h to re-generate the photocatalyst.

3. Results and discussion

The crystalline structure of the as-fabricated samples has been characterized by XRD technique. The XRD patterns of the samples fabricated at 150 °C, 250 °C, 350 °C, 450 °C, 550 °C and 650 °C calcination temperature respectively as shown in Fig. 1. The sample treated at 150 °C revealed to be amorphous because having no diffraction peak in crystallographic measurement. While two very weak diffraction peaks of crystalline AgBr at 30.7° and 44.05° has been recorded at 250 °C, can be indexed to (200) and (220) crystal planes, while there is no peak of Ag and TiO_2 at this temperature. Similarly the sample treated at 350 °C and 450 °C has diffraction peaks at 31.05°, 44.57° and 54.79° corresponds to (200), (220) and (222) (JCPDS Card No.65-2871) of AgBr crystal respectively, and at 64.33° correspond to (204) (JCPD card NO. 21-1272) of anatase TiO_2 crystal [24,25], in addition one new peak at 38.85° (JCPDS Card No. 04-0783) of Ag(111) nano particles also appeared at 450 °C. Whereas the XRD results of the sample calcined at 550 °C and 650 °C have very intense peaks at 21.98° correspond to (002) of SiO_2 (JCPDS card NO. 15-26), 25.68°, 48.90° and 64.33° correspond to (101), (200) and (204) (JCPD card NO.21-1272) of pure anatase TiO_2 [25]. Similarly the peaks at 38.85° and 44.61° and 64.65° are the diffraction results of face centered cubic crystal of Ag (111) and (200) and (220) (JCPDS Card No. 04-0783) and at 31.56°, 44.57°, 56.36° (200), (220) and (222) (JCPDS Card No. 65-2871) correspond to AgBr respectively [24]. It is evidently found that by increasing the calcinations temperature, the samples revealed much sharper peaks, which ascribed the formation of characteristics crystalline nature of nano composite that composed of Ag and AgBr nano particles and anatase phase of titania. other than it has been reported formerly that above 600 °C, there is phase transition from anatase to rutile phase of titania and up to 900 °C it is completely transferred into rutile phase [26].

Moreover, for comparative studies the X-rays diffraction results of HHST, Ag-AgBr and Ag-AgBr/HHST obtained at optimum calcination temperature and (Degussa P25) was also carried out and displayed in Fig. 2. It was observed that the XRD diffraction results of Ag-AgBr has close resemblance to Ag-AgBr/HHST excluding the peak at 38.1° (111) of FCC plane of Ag. This might be attributed to the silica-titania support that import great influence on crystalline structure of Ag-AgBr/HHST [20,27,28].

and structural information has been explored by SEM and HRTEM analysis of uncovered HHST and Ag-AgBr/HHST obtained at 550 °C. The SEM images of both the samples shows that it possesses hollow structure with spherical spheres that are constructed by small spheres@ large spheres. In case of HHST the shells of big spheres is composed of small spheres having smooth surfaces, while in Ag-AgBr/HHST all the spheres are rough and have regular get in touch with each other due to loading of Ag and AgBr nano particles (Fig. 3).

The HRTEM images of the HHST, and Ag-AgBr/HHST nano composite synthesized at 550 °C and Ag-AgBr/HHST at 650 °C as shown in Fig. 4. The outer surfaces of the HHST nano spheres is to some extent smooth, having TiO_2 coated SiO_2 hollow spheres while the interior of the hollow spheres have rough surfaces, because the whole nano spheres consist of a large number of small hollow spheres about 10–20 nm, and construct a big hollow spheres, about 70–150 nm (Fig. 4a). It was found that the surfaces of most of the hollow spheres

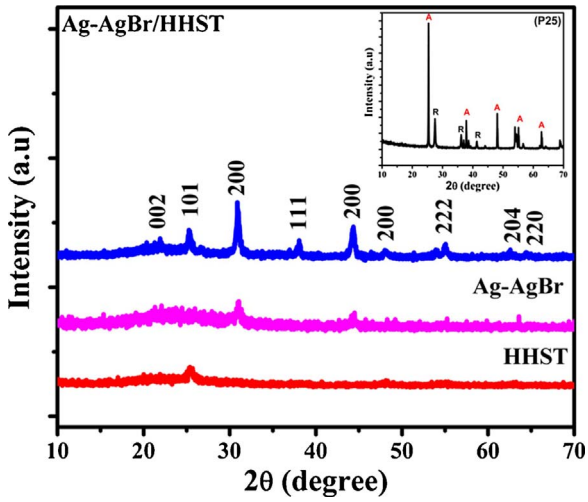

Fig. 2. XRD pattern of HHST, Ag-AgBr and Ag-AgBr/HHST synthesized at optimum calcination temperature, while inset is the XRD spectra of (Degussa P25).

retained their spherical symmetry, and have close intact with other spheres with a lot of cavities. While in case of Ag-AgBr/HHST surfaces as well as hollow interior of the composites that can evidently examine from the broken edges is not smooth because of the Ag and AgBr nano particles in the form of black dots (2–8 nm) that are regularly distributed with no aggregation on the surface of HHST, that confirms the combination of HHST spheres with the Ag and AgBr nano particles (Fig. 4b&c). Most of the particles are deeply embedded, these very small sized Ag-AgBr nano particles was strongly attached and stabilized at the HHST surface. It is very complicated to visibly point out the position of Ag and AgBr nanoparticles in Ag-AgBr/HHST because AgBr can decomposed easily under ultra violet light during photolysis [20]. Whereas the sample obtained at 650 °C has particle size larger than at 550 °C, the reason behind this is the aggregations of smaller particles to form a larger one by increasing the temperature from 550 °C to 650 °C (Fig. 4b) [29].

The lattice fringes with the spacing of d = 0.23 nm correspond to (111) crystallographic plane of Ag, and d = 0.34 nm lattice spacing correspond to (101) of anatase TiO_2 seems an interfacial contact has established between Ag and TiO_2 species to build up a heterostructure (Fig. 4d). It is concluded from the SEM and HRTEM measurements that Ag-AgBr/HHST revealed a hollow hierarchical spherical morphology and loose structures consist of abundant nano particles that regularly dispersed on the surface of HHST support. This distinctive morphology is very cooperative throughout photocatalytic degradation process.

The elemental compositions of Ag-AgBr/HHST synthesized at optimum calcination temperature was studied by EDS and displayed in Fig. 5a. The results illustrated that sample contains Ag, Br, Si, Ti and O, correspond to more validate the existence of Ag and AgBr nano particles on the surface of HHST. The SEM elemental mapping of the nano composite shown in Fig. 5b.

The Nitrogen adsorption-desorption isotherms and the BJH pore size distribution curve of Ag-AgBr/HHST, HHST and Ag-AgBr respectively shown in Fig. 6. It was observed that all the photo catalysts exhibit the typical IV type isotherm, which is the characteristic feature of the mesoporous materials. The hysteresis loop for all the photo catalysts is of type H_3, undoubtedly signifying the slit like pores of the material. There are two hysteresis loops in Ag-AgBr/HHST curve indicated the amount of adsorption increased more appreciably at relative pressure $0.4 < P/P_0 < 0.9$ considered as filling of nitrogen gas in hollow voids. This is due to larger surface area that promoting monolayer nitrogen adsorption towards the walls of mesopores [30]. In adding together the Ag-AgBr/HHST desorption curve is somewhat narrow indicated that size of the mesopores is extra homogeneous. Similarly the pore size distribution of Ag-AgBr/HHST, HHST and Ag-AgBr comprise an average sizes of 7.72 nm, 6.40 nm and 4.66 nm respectively as shown in insets (Fig. 6). The larger pore sizes and total volume of Ag-AgBr/HHST is attributed to the ordered dispersion of tiny Ag and AgBr nano particles on the walls of the pores that solidify the walls and suppress the structure collapse of the mesoporous HHST. This phenomenon demonstrated that the incorporation of Ag and AgBr nano particles on HHST surface are involved in the formation of the pores, while did not block and destroy the mesoporous structure of the material at optimum calcination temperature, because Ag-AgBr/HHST was prepared by adding CTAB and AgBr so when the samples were calcined and radiate under UV light for 60 min, which accelerate the breakdown of CTAB and the photolysis of AgBr to reduce partially Ag^+ to Ag^0 .The space occupied by CTAB and AgBr is empty, which make the $BET_{(s.a)}$, pore sizes and total volume of Ag-AgBr/HHST are larger than Ag-AgBr and HHST [20,31,32]. The textural properties of Ag-AgBr/HHST, HHST and Ag-AgBr are summarized in Table 1.

The optical properties were investigated by UV–vis. diffuse reflectance spectroscopy. The UV–vis. DR. spectra of Ag-AgBr/HHST(T-1), Ag-AgBr/HHST(T-2), Ag-AgBr/HHST(T-3), Ag-AgBr/HHST(T-4), Ag-AgBr/HHST(T-5) and Ag-AgBr/HHST(T-6) nano composites synthesized at 150 °C, 250 °C, 350 °C, 450 °C, 550 °C and 650 °C respectively as displayed in Fig. 7a. The outcomes of the absorption studies shows that Ag-AgBr/HHST(T-5) and Ag-AgBr/HHST(T-6), absorb the light strongly in the visible as well as in ultra violet region and be evidence for strong absorption bands than Ag-AgBr/HHST(T-1), Ag-AgBr/HHST(T-2), Ag-AgBr/HHST(T-3) and Ag-AgBr/HHST(T-4). This is due to the amorphous nature at this lower temperature or due to crystal defect in later compounds. The high absorbance of Ag-AgBr/HHST(T-5) and Ag-AgBr/HHST(T-6) in visible light region can be attributed to the visible light responses of Ag and AgBr [33–35]. Whereas

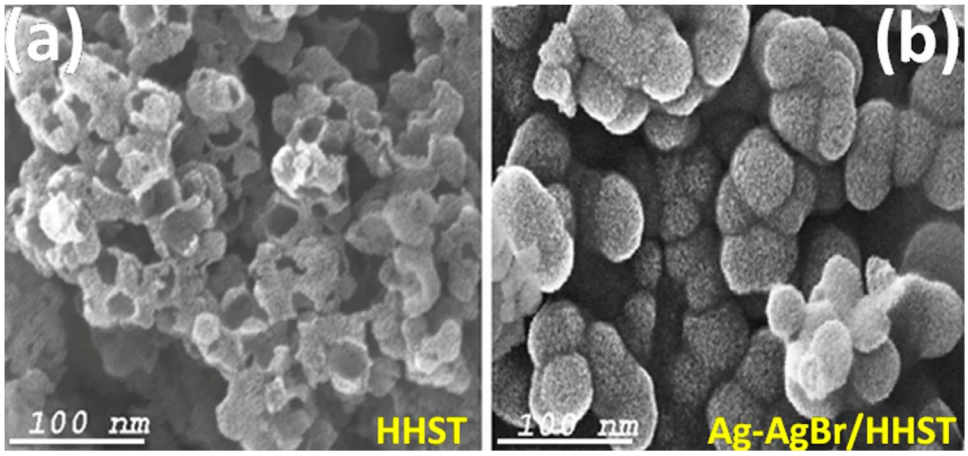

Fig. 3. SEM image of (a) hollow hierarchical silica-titania act as support (b) Ag-AgBr/HHST nano composite synthesized at optimum calcination temperature.

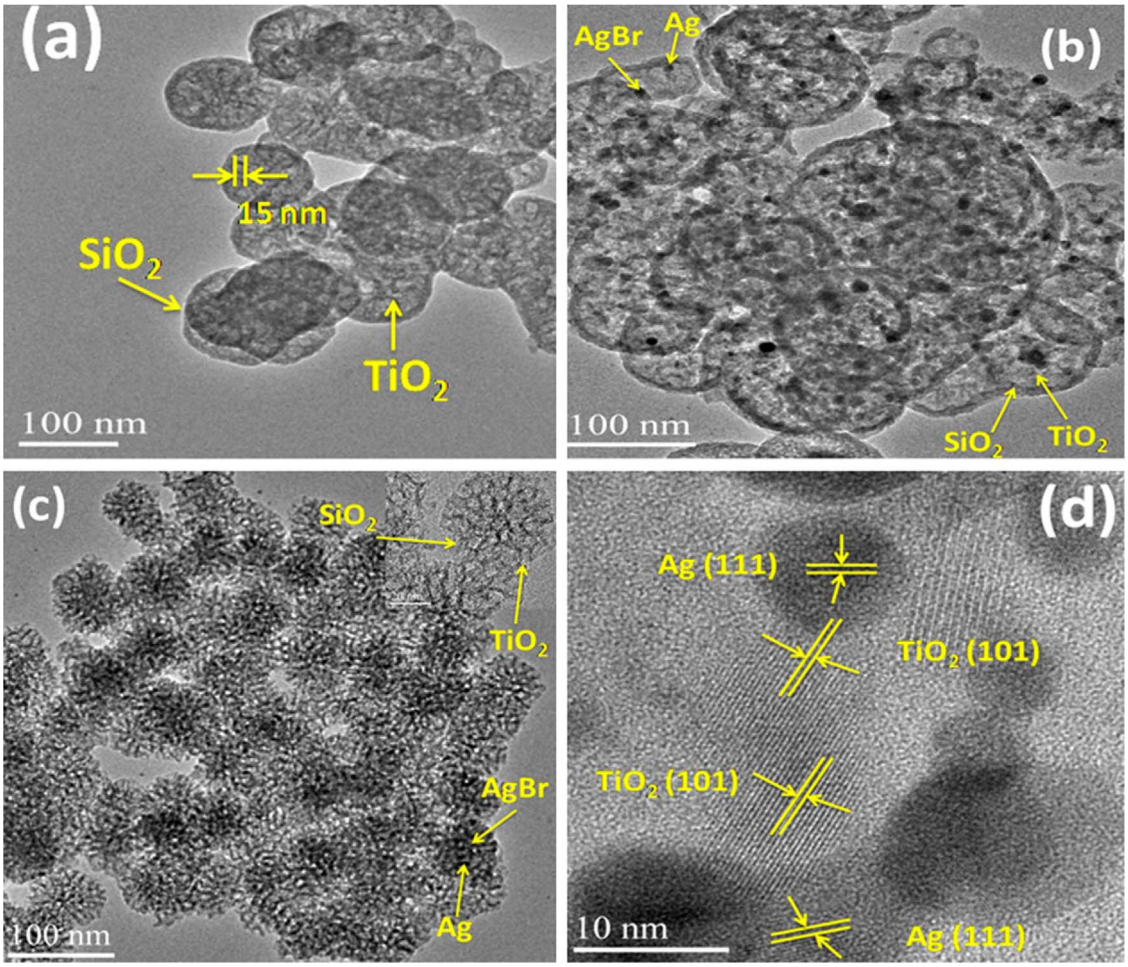

Fig. 4. (a) HRTEM image of HHST, (b) Ag-AgBr/HHST prepared at 650 °C, (c & d) Ag-AgBr/HHST prepared at optimum calcination temperature.

the absorption in ultra violet region contributed by pure anatase phase of titania. The absorption in ultra violet region have a little dramatic variations, Ag-AgBr/HHST(T-5) strongly absorb the light in ultra violet region than Ag-AgBr/HHST(T-6), because of pure anatase phase of TiO_2 as discussed in XRD and HRTEM measurements. Consequently due to unusual assembly of Ag-AgBr and silica-titania boost the combine

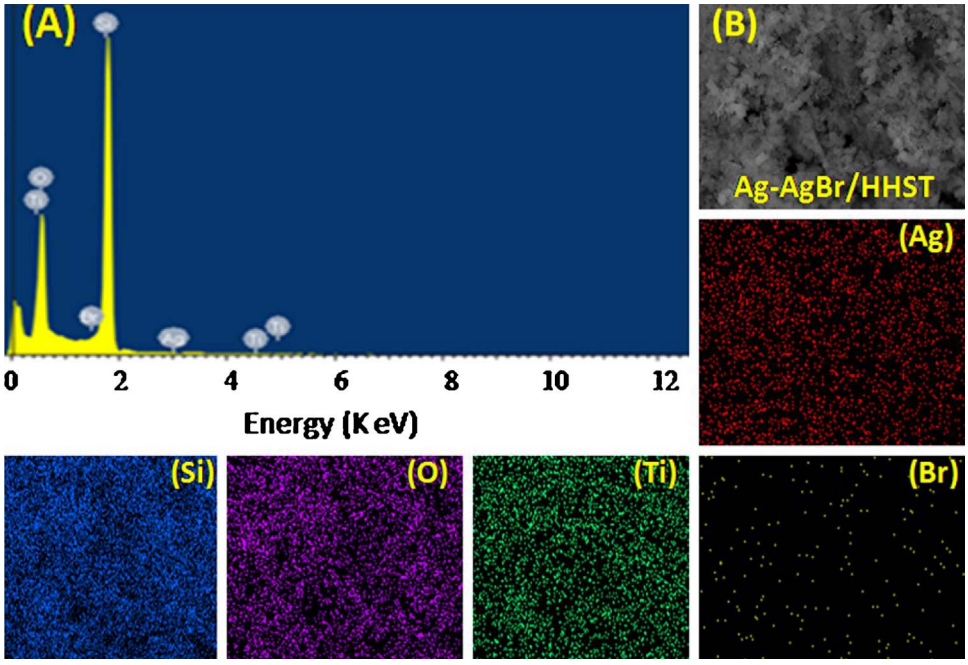

Fig. 5. (a) EDS analysis and (b) elemental mapping of Ag-AgBr/HHST synthesized at optimum calcination temperature.

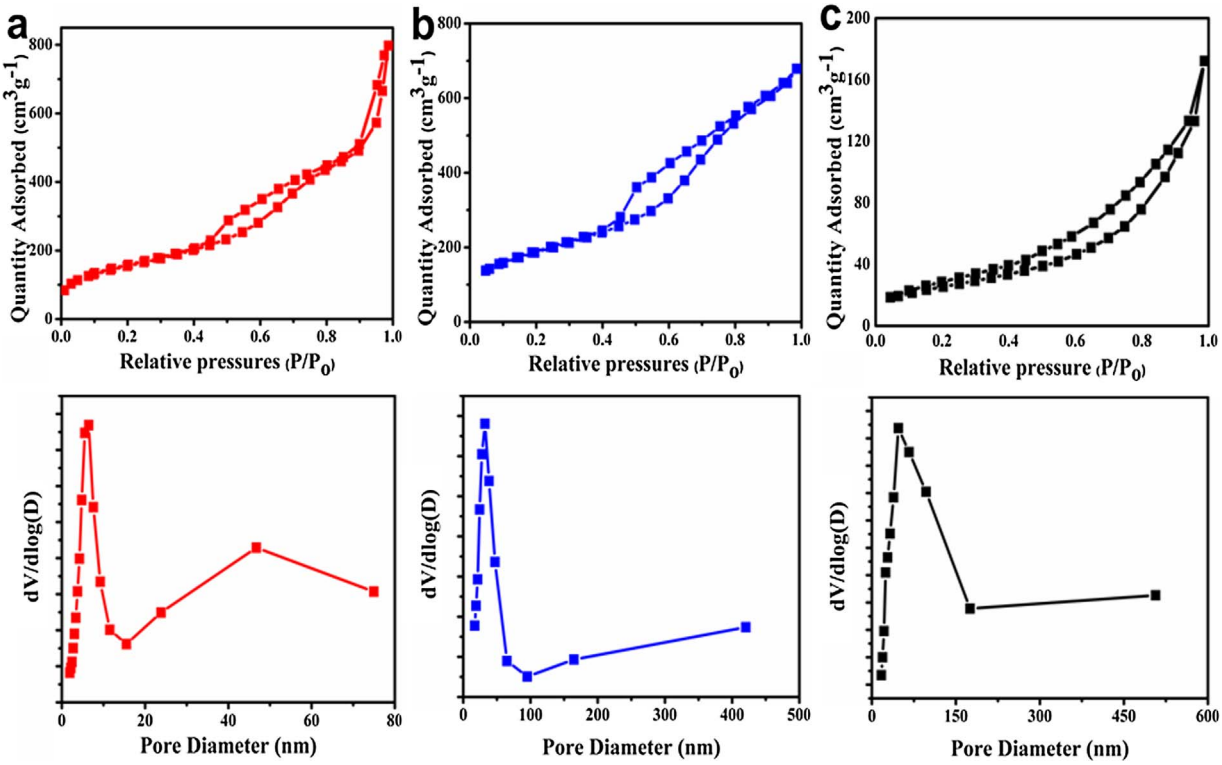

Fig. 6. Nitrogen adsorption-desorption Isotherm and inset BJH pore size distribution curve of (a) Ag-AgBr/HHST (b) HHST and (c) Ag-AgBr prepared at optimum calcination temperature.

Table 1
The surface textural properties of Ag-AgBr/HHST, HHST and Ag-AgBr.

Photocatalyst	SBET (m^2g^{-1})	Mean pore size (nm)	Total volume (cm^3g^{-1})
Ag-AgBr/HHST	652.21	7.72	1.05
HHST	572.76	6.40	1.02
Ag-AgBr	106.84	4.66	0.95

localized surface plasmonic resonance outcomes, absorb the light stoutly in visible as well as ultra violet region [36,37]. Similarly the UV–vis. DR. spectra was also taken in the range of 220–750 nm for the P25, HHST, Ag-AgBr and Ag-AgBr/HHST synthesized at optimum calcination temperature (Fig. 7b). The absorption spectra of (Degussa P25) exhibits the fundamental absorption peak only in the UV region, assign to absorption edge approximately 375 nm (Eg = 3.22 eV), indicated that there is no more absorption in visible light region. While HHST absorbed the visible light to some extant with absorption edge approximately 400 nm (Eg = 3.12 eV), similarly Ag-AgBr also absorb the visible light to some extent. Whereas the Ag-AgBr/HHST has extra wide and significant enhancement of light absorption even at whole the visible light range of 400–750 nm, this might be attributed to SPR effect of Ag NPs and synergetic effects between the Ag, AgBr and TiO_2, demonstrating that it possesses high-quality effectiveness and applicability as a visible and UV light driven photocatalyst [38,39]. For crystalline semiconductors, the optical absorption near the band edge was calculated by the $E_g = 1240/\lambda$, where λ is the onset absorption wavelength. The band gap of Ag-AgBr/HHST heterostructure confirm

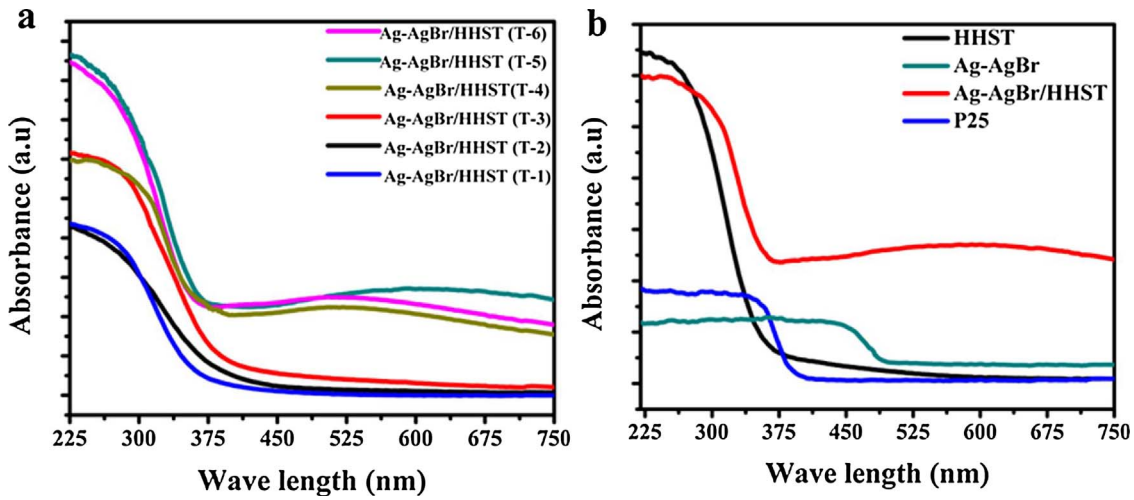

Fig. 7. UV–vis absorption spectra of various sample synthesized at different calcination temperature (a) Ag-AgBr/HHST(T-1) at 150 °C, Ag-AgBr/HHST(T-2) at 250 °C, Ag-AgBr/HHST(T-3) at 350 °C, Ag-AgBr/HHST(T-4) at 450 °C, Ag-AgBr/HHST(T-5) at 550 °C, and Ag-AgBr/HHST(T-6) at 650 °C. (b) UV–vis. absorption spectra of different samples synthesized at optimum calcination temperature.

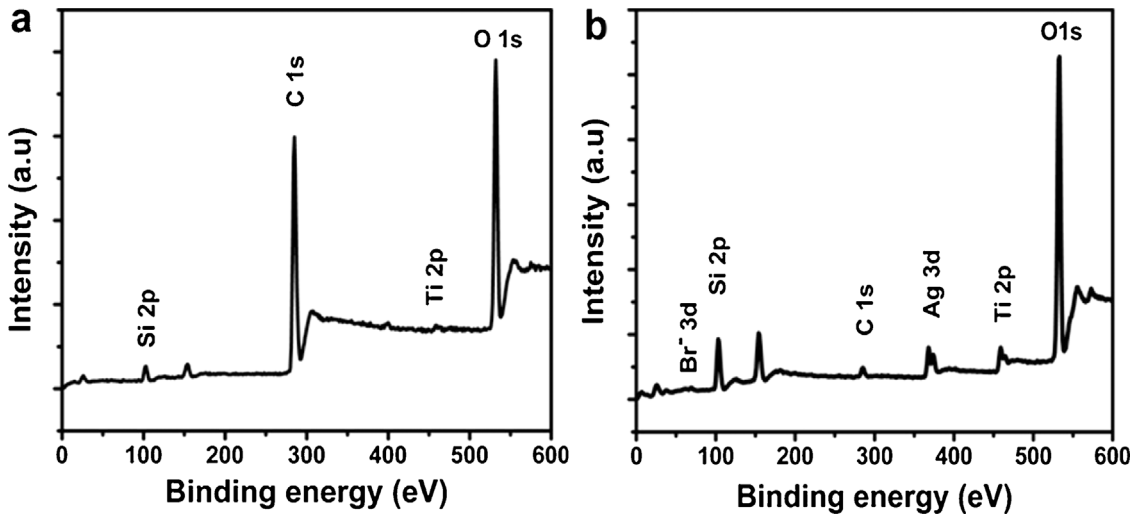

Fig. 8. High resolution XPS spectra survey for (a) HHST, (b) Ag-AgBr/HHST hollow hierarchical mesoporous nano composite synthesized at optimum calcination temperature.

the red shift of the absorption edge about 614 nm (2.11 eV) [30]. The extending of absorption edges probably led to the superior photocatalytic efficiency under simulated irradiated light. In addition, as the Ag-AgBr/HHST nano composite effectually absorb the UV and visible light, so such type of nano composite has superior photocatalytic proficiency for colored compounds under visible light and for colorless compound under UV light irradiations, due well matching in frequency that responsible for electronic excitation.

The surface properties and chemical composition of HHST and Ag-AgBr/HHST was determined by X-rays photoelectron spectroscopy. The peaks appeared in the survey spectra correspond to their elemental composition (Ag, Br, Ti, Si and O) except C 1 s peak 284.82 eV from hydrocarbon in the XPS instrument (Fig. 8). The XPS results of Ti, confirms the peak position of Ag-AgBr/HHST shifted to higher binding energy than uncovered HHST support (Fig. 9a). It indicates the lower electron density of Ti atom in the Ag-AgBr/HHST confirm strong interaction between Ag and AgBr nano particles. Furthermore it was observed that the peak of Ti $2p_{3/2}$ of Ag-AgBr/HHST could be fitted into two bands, at 458.76 eV, ascribed to Ti(III), and at 459.50 eV, ascribed to Ti(IV), that also justify the strong interaction between Ag and AgBr with TiO_2 (Fig. 9b), while no inside peak was observed in uncovered HHST. The Ti(III) oxide has a narrow band gap because its energy level is located between the conduction band and valence band of TiO_2, which might be considered more effective for superior photocatalytic activity of the Ag-AgBr/HHST under visible as well as UV light irradiations [40,41]. The XPS results of Ag 3d of Ag-AgBr/HHST are displayed in (Fig. 9c). The results indicated that two bands of Ag $3d_{5/2}$ and Ag $3d_{3/2}$ could be further divided into four different peaks, the peak Ag $3d_{5/2}$ at 368.15 eV and Ag $3d_{3/2}$ 374.05 eV are of Ag^+, while at 368.90 eV and 374.95 eV attributed to Ag^0 nano particles, similarly peak of Br $3d_{5/2}$ and Br $3d_{3/2}$ with the binding energies of 68.35 eV and 69.32 eV [28,42] (Fig. 9d). Noticeably binding energy of the Ag-AgBr/HHST observed higher than reported individual Ag-AgBr, this improvement to higher energy, indicated its stability correspond to the strong attraction with the silica-titania [30]. Hence, the joint characterization of XRD and XPS confirms the co-existence of Ag and AgBr nano particles on the surface of HHST and encompass well-built connection with each other, which verify that electronic transportation takes place from TiO_2 to metallic Ag then to AgBr that help to separate the photo excited electron-hole pairs, while the hollow hierarchical mesoporous structure also slow down the recombination rate of excited electrons and holes and hence boost its photocatalytic activity [43,44].

To determine the charge separation and electron hole pair recombination rate of the as-fabricated nano composites, the PL measurements was carried out. The PL spectra of the Ag-AgBr/HHST, HHST and P25 shown in Fig. 10a. It is evident that the P25 and HHST gave broad band with high intensity PL signals assigned to the radiative recombination of self-trapped excitation. Whereas the PL spectra of the Ag-AgBr/HHST heterostructure exhibited almost quenched inferior intensity emission spectrum, which imply more efficient charge transfer and maintained longer life time of electron-hole pair separation [45–47]. Similarly to examine the conductivity and its correlation with the rate of photo generated charge transfer and their recombination behavior for Ag-AgBr/HHST, Ag-AgBr and HHST, the EIS measurements was carried out in the three-electrode system in 1 M KOH as displayed in Fig. 10b. The EIS results of Ag-AgBr/HHST indicated that the impedance spectrum exhibited a smaller radius and very small charge transfer resistance (22.5 Ω) than Ag-AgBr (98.5 Ω) and HHST (105.5 Ω) that correlated with enhanced conductivity, which is responsible for superior charge transfer and lower recombination rates of photo generated charges during photo catalysis. This is due to synergetic coupling of Ag and AgBr with hollow hierarchical silica-titania that make available high surface area with exposed active site that facilitate the charge transfer during the photocatalytic reaction [48,49].

The transient photocurrent responses vs time was also carried out to added more demonstration about the transfer and recombination behavior of charges during photo catalysis. Higher the photo-current indicates enhancement in the charge transfer and decrease the recombination rate of electron-hole pairs (Fig. 11). The progression of photocurrent was investigated as Ag-AgBr/HHST > Ag-AgBr > HHST. This might be attributed to the unique hollow hierarchical heterostructure as well as the combination of Ag, AgBr and TiO_2. In addition the immediate amplification of the photocurrent from off to on state proves the existence of photo anodes that are receptive to illuminated light added more effectiveness for the generation and separation of electron-hole pairs [50].

4. Photocatalytic performance

The potential photocatalytic activity of the selected samples synthesized at optimum calcination temperature has the immense environmental significance. The degradation of organic pollutants by metal/metal halide and metallic oxides heterostructure photocatalyst is most meaningful indeed. A variety of industries discharge assortment of dyes to the aqueous environment that are very hazardous to the living wage. It has been predictable that 10–50% of the dyes has been thrown into the environment during the dye. Among all these methyl orange and aniline are the effectual dyes used as coloring agent in textile and paper industries. Thus, the photocatalytic activity of the as-prepared Ag-AgBr/HHST, Ag-AgBr and HHST and Degussa P25 was investigated

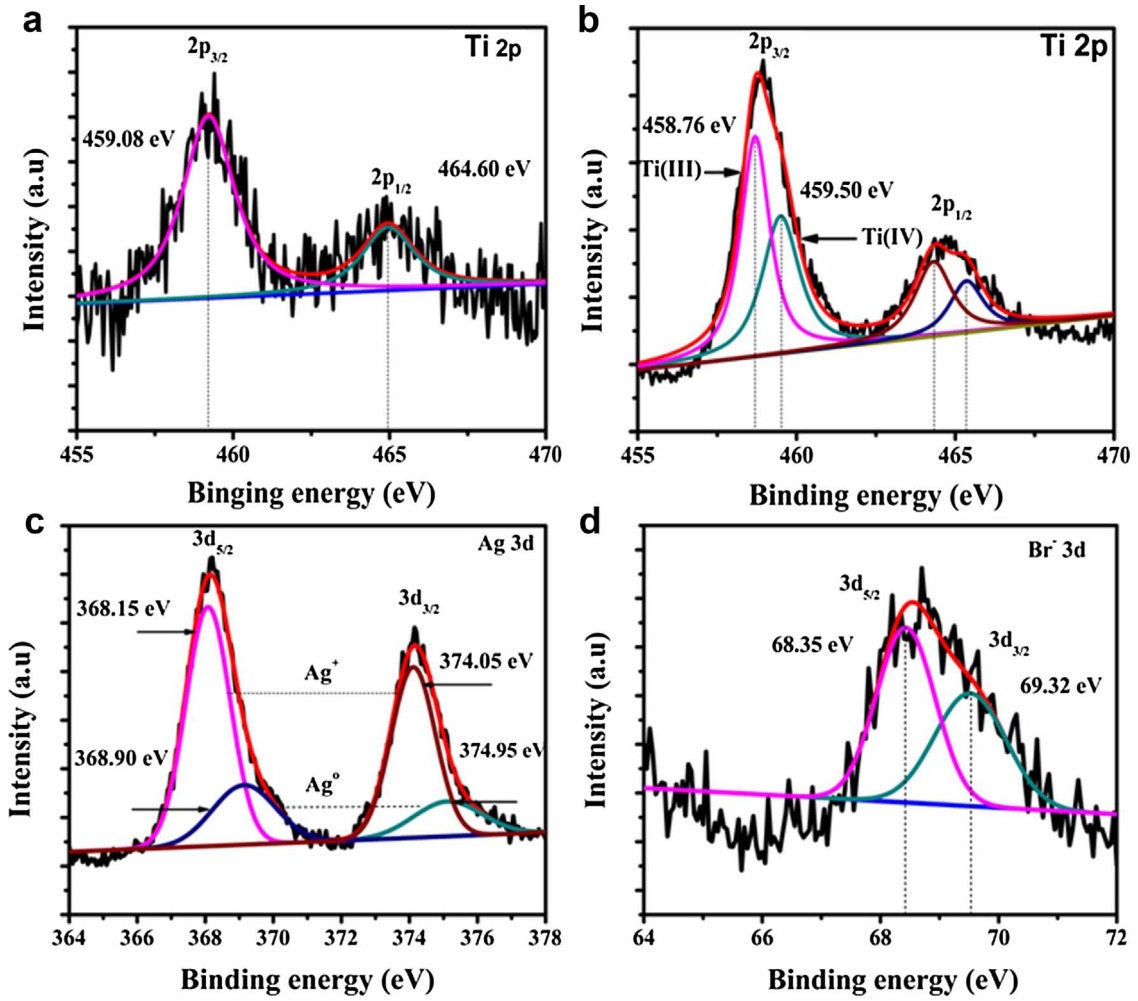

Fig. 9. High resolution XPS spectra (a) Ti2p of uncovered HHST (b) Ti2p of Ag-AgBr/HHST (c&d) Ag3d and Br3d of Ag-AgBr/HHST hollow hierarchical mesoporous nano composite synthesized at optimum calcination temperature.

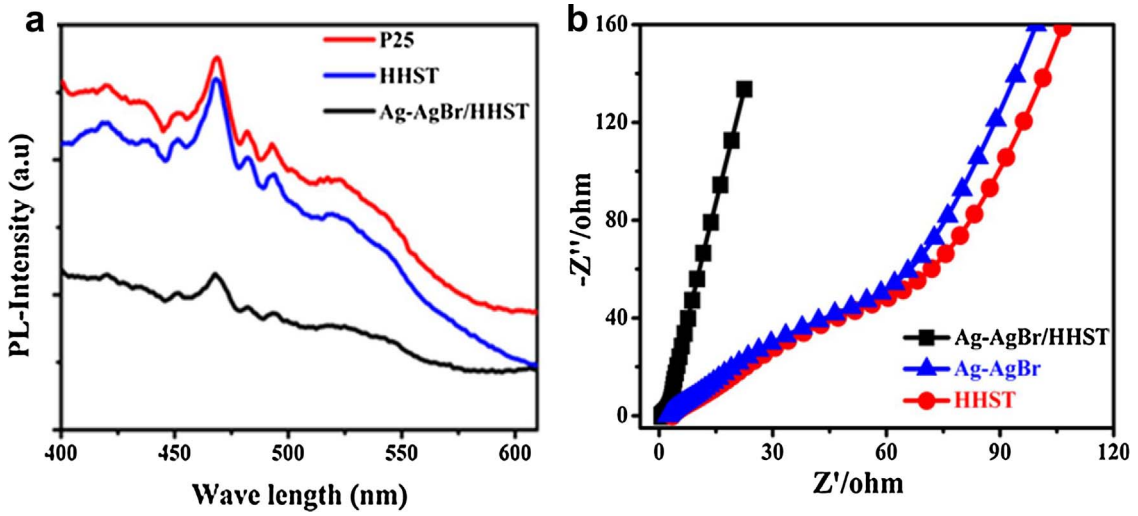

Fig. 10. PL Emission spectra of the (a) P25, HHST and Ag-AgBr/HHST synthesized at optimum calcination temperature. The spectra was taken at excitation wave length of 360 nm. (b) EIS spectrum of Ag-AgBr/HHST, Ag-AgBr and HHST.

by the degradation of 200 mL(200 ppm) methyl orange and aniline aqueous solutions, when exposed to ultra violet and visible light for various time intervals (Figs. 12 and 13). It is obvious that an adsorption-desorption equilibrium have to developed between the photo catalysts and organic pollutants for 30 mn in dark with steady stirring, revealed that the concentration of methyl orange decreased by Ag-AgBr, HHST and Ag-AgBr/HHST, (2.5%), (5.2%) and (10.2%), while aniline (3.7%), (4.2%) and (8.3%) respectively due to adsorption of dyes on the surface of the photocatalysts. The amount of dyes adsorption rises in order by increasing tendency of the surface area and total

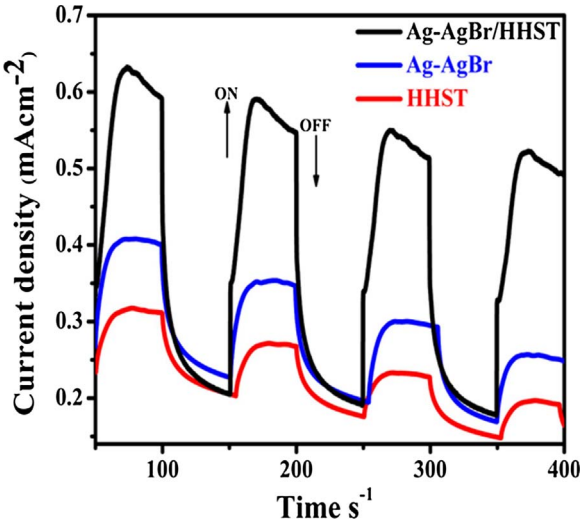

Fig. 11. Photo-current density under illuminated light and in dark of Ag-AgBr/HHST, Ag-AgBr and HHST.

pore volume. It can be observed that pure HHST and Ag-AgBr has lesser adsorption ability than Ag-AgBr/HHST nano composite. This is due to the high surface area, high total volume and unusual hollow hierarchical structure of the Ag-AgBr/HHST that offer appropriate space for the mass transport. The adsorption of the pollutants on the surface of photocatalyst highly correlated with the latter photo degradation. The percent photocatalytic degradation capability of Ag-AgBr/HHST for methyl orange report 21.75, 2.18 and 2.49 times superior under UV light and 2.2, 4.3 and 66.0 times superior under visible light than the corresponding Ag-AgBr, HHST and P25 respectively. Whereas for aniline degradation Ag-AgBr/HHST report 25.71, 3.33 and 5.63 times superior under UV light and 2.0, 3.8 and 76.0 time superior under visible light than the corresponding Ag-AgBr, HHST and P25 respectively. A blank experiment was also run analogous to photocatalysts which shows that degradation without catalyst was insignificant and the concentration of the dyes after irradiations was unaffected, indicating the stability of organic pollutants under the simulated ultra violet and visible light. The batter photocatalytic activity of Ag-AgBr/HHST towards the degradation of methyl orange than aniline under visible light irradiations reflects the extra stable and inert electronic structure of aniline, accredited to Л-conjugated molecular structure. While the high visible light photocatalytic degradation of methyl orange possibly suggested by self-photosensitization of methyl orange molecules interacted with Ag-AgBr/HHST nano composite, because the methyl orange molecule can be excited under visible light irradiations due to well matching in frequency, which leads to electrons injection from the adsorbed dye species to the Ag-AgBr/HHST where it react with the surface adsorbed O_2 molecules to yield reactive oxygen species [51,52]. While the superior photocatalytic degradation activity of Ag-AgBr/HHST than the individual Ag-AgBr and HHST can be attributed to the formation of the heterostructure that hold synergetic effect between Ag and AgBr with TiO_2 on the surface of silica-titania. The

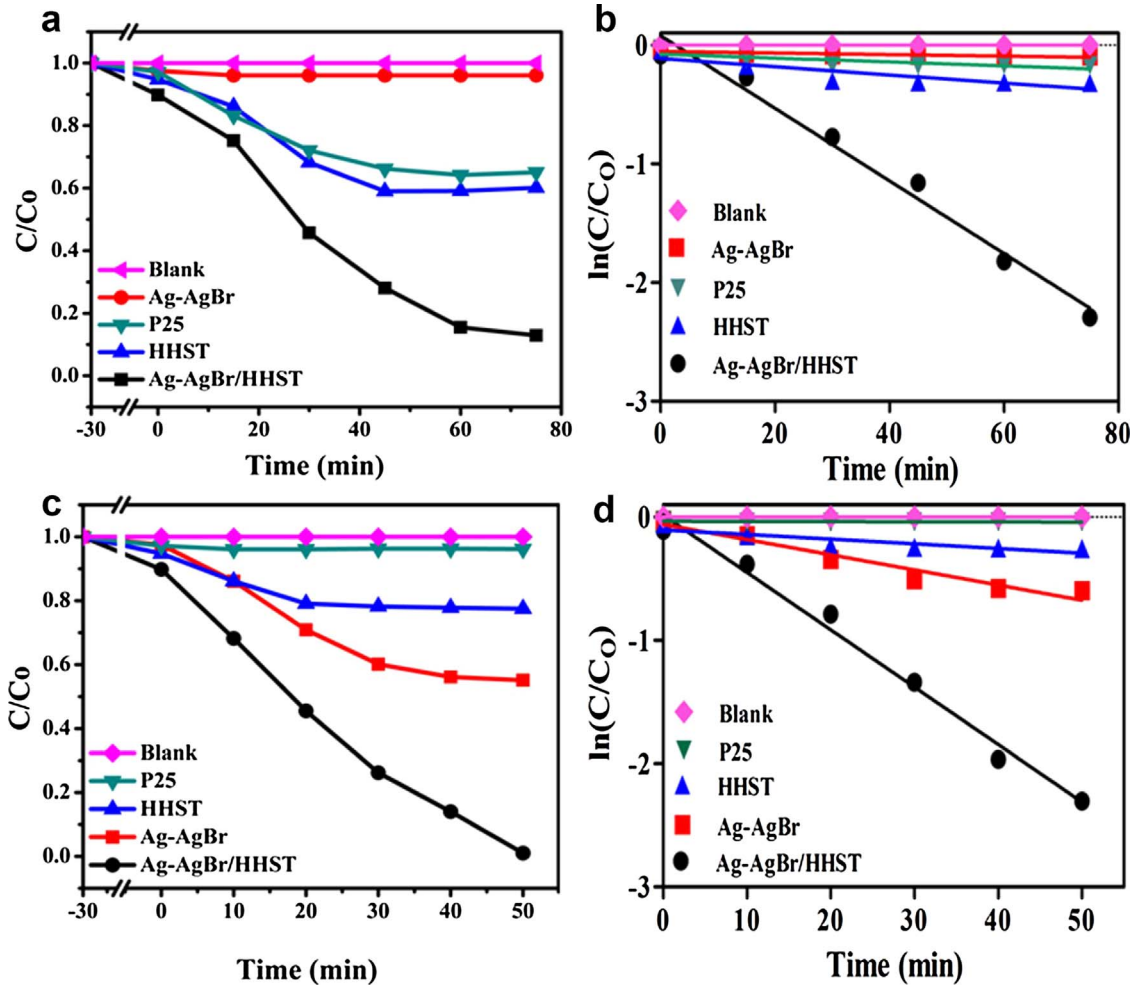

Fig. 12. (a&c) Photocatalytic degradation activity of Ag-AgBr/HHST and reference samples, (b&d) first order kinetic plots, under irradiated ultra violet and visible light respectively, as a function of irradiation time using 0.2 g sample weight and 200 mL (200 ppm) aqueous solution of methyl orange.

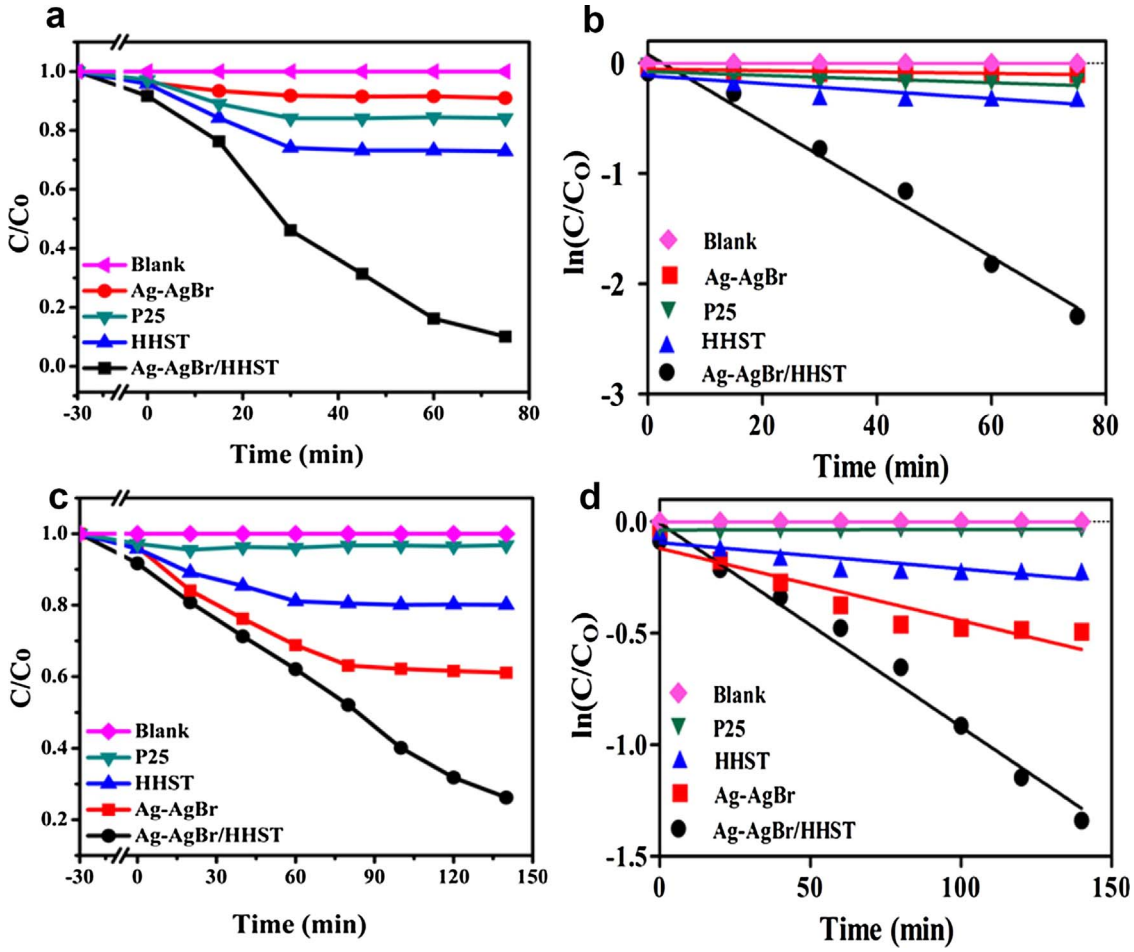

Fig. 13. (a&c) Photocatalytic degradation activity of Ag-AgBr/HHST and reference samples, (b&d) first order kinetic plots, under irradiated ultra violet and visible light respectively, as a function of irradiation time using 0.2 g sample weight and 200 mL (200 ppm) aqueous solution of aniline.

Table 2
Photocatalytic degradation activity of Ag-AgBr/HHST and reference samples for methyl orange and aniline.

	(%)Photocatalytic degradation for methyl orange 200mL(200 ppm)		(%)Photocatalytic degradation for Aniline 200mL(200 ppm)	
Catalyst (0.2 g)	UV light	Visible light	UV light	Visible light
Ag-AgBr/ HHST	87.0	99.0	90.0	76.0
Ag-AgBr	4.0	45.0	3.5	38.0
HHST	40.0	23.0	27.0	20.0
P25	35	1.5	16	1

Table 3
Kinetic rate constant of Ag-AgBr/HHST and reference samples during photocatalytic degradation reaction.

	Kinetic rate constant, k(mn^{-1}) for Methyl Orange 200mL (200 ppm)		Kinetic rate constant, k(mn^{-1}) for Aniline 200mL(200 ppm)	
Catalyst (0.2 g)	UV light	Visible light	UV light	Visible light
Ag-AgBr/ HHST	0.0306	0.0465	0.0306	0.0091
Ag-AgBr	0.0007	0.0123	0.0007	0.0032
HHST	0.0034	0.0038	0.0034	0.0012
P25	0.0017	0.0001	0.0017	0.00003

photocatalytic degradation results summarized in Table 2.

The kinetic study for the degradation of methyl orange and aniline was carried out by fitting the experimental data in rate equation ($-\ln(C_t/C_o) = kt$), where k is the first-order rate constant. The kinetic data curves of photocatalytic degradation of methyl orange and aniline displayed in (Fig. 12 and 13) respectively. The linear relationship between $\ln(C/C_o)$ and irradiation time demonstrated that the photocatalytic degradation reaction follows pseudo-first-order kinetics [53]. The rate constants (k) for methyl orange and aniline photocatalytic degradation, declare to be higher for Ag-AgBr/HHST heterostructure than the individual components under UV and visible light irradiations ensure higher photocatalytic capabilities (Table 3).

The stability of Ag-AgBr/HHST is an imperative subject for long term existence and repetitive use in practical applications. The recycling experiments were conducted to examine the stability of the hollow mesoporous compound under the same circumstances (Fig. S1). It is observed that, the elimination rates of methyl orange and aniline by Ag-AgBr/HHST still remain high after five cycles under visible light irradiations, while a minute change was observed in percent degradation rate under UV light because of the photolysis of AgBr while exposed for a long time throughout the degradation of organic dyes, which indicate that the material can stay itself stable after many repetitive cycles.

The crystalline structure of the Ag-AgBr/HHST after five degradation cycles was investigated by XRD measurements (Fig. S2), it shows that, in recycled photocatalyst the position of the peaks almost similar as in fresh sample. Furthermore the SEM, EDS with elemental mapping

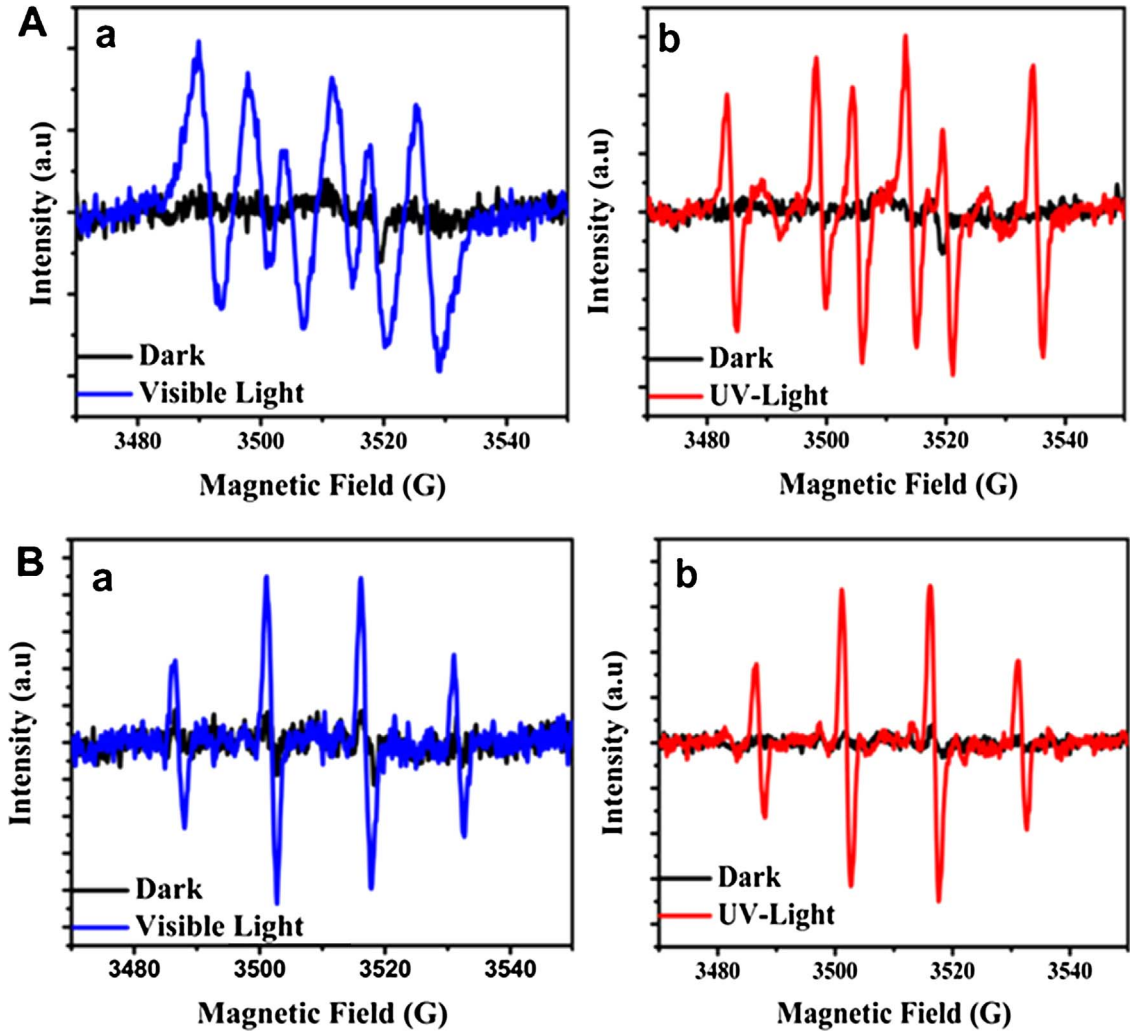

Fig. 14. (A) DMPO-$O_2\cdot^-$ spin-trapping EPR spectra recorded at ambient temperature in methanolic dispersion under (a) visible light (b) UV light, (B) DMPO-·OH spin-trapping EPR spectra recorded at ambient temperature in aqueous dispersion under (a) visible light (b) UV light. The signals were recorded after visible and UV light irradiation of 40 s for Ag-AgBr/HHST.

and BET analysis was also carried out (Figs. S4 and S5), the outcomes indicated that the photocatalyst has still hollow hierarchical mesoporous heterostructure having consistent distribution of particles, and prevents any components being misplaced that results in the protection of excellent photocatalytic activity and structural stability after five consecutive photocatalytic degradation cycles.

4.1. Mechanism of the photocatalytic degradation

On the basis of the outcomes of the photocatalytic degradation results, the possible mechanism for the elevated stability and superior photocatalytic activity of the Ag-AgBr/HHST for the degradation of organic pollutants under simulated light, could be attributed to the combination of HHST nano spheres, Ag and AgBr nano particles, that could promote more rapid transfer of electrons and holes among AgBr, TiO_2 and Ag NPs via hollow hierarchical silica spheres, and avoided the recombination of the excited electrons and holes, hence accelerate the photo degradation process [54–56]. Consequently, the appropriate reactions taking place at the surface of composite involved in the degradation process. In the Ag-AgBr/HHST nano composite system, both the TiO_2 and AgBr can be excited by the simulated solar light having different photo-absorption ranges, so can enhance the utilization of the solar light simulation. A schematic illustrations of the band levels of the Ag-AgBr/HHST composite and the possible reaction mechanism of the photocatalytic procedure is given in Fig. S8. Under the simulated solar light irradiations, the electrons in the valence band (VB) of TiO_2 and AgBr are excited to their corresponding conduction band (CB). Then the electrons in the (CB) of TiO_2 migrate into the metallic Ag (electron transfer I: TiO_2 to Ag) across the schottky barrier because the (CB) of TiO_2 is higher compare to the loaded metallic Ag, This process of electron transfer is faster than the electron-hole recombination between the (VB) and (CB) of TiO_2. Thus the electrons in the (CB) of TiO_2 can be stored in the Ag component. Meanwhile, because the energy level of Ag is above the (VB) of AgBr, the holes in the (VB) of AgBr can also easily flow into metallic Ag (electron transfer II: Ag to AgBr), which is faster than the electron-hole recombination between the (VB) and (CB) of AgBr. Therefore, instantaneous electron transfer I and II should occur as a result of simulated solar light excitation of both TiO_2 and AgBr, which is similar to previous reports [57,58]. As a result, the holes in the (VB) of TiO_2 with a strong oxidation power can take a part in photocatalytic reactions to directly degrade the organic pollutants, and the electrons in the (CB) of AgBr with a strong reduction power can be transferred to the adsorbed O_2 acting as an electron acceptor to form first the superoxide radical anions $O_2\cdot^-$. While other oxidative species such as ·OH etc. would be further produces from $O_2\cdot^-$ free radicals[59]. These active species will result in the degradation of organic dyes. Furthermore, during the reaction Ag NPs shows dipolar plasmonic reaction using the visible light irradiations, the electrons from the plasmon-excited Ag

nanoparticles transferred to the CB of AgBr. The $O_2\cdot^-$ radicals were generated by O_2 trapping the electron in the (CB) of AgBr coming from both the photo excited AgBr and plasmon-photo excited Ag nanoparticles. Therefore, the efficient degradation of organic dyes came from both the photo excited AgBr and plasmon-excited Ag nanoparticles. The transfer of electron from plasmonic Ag NPs to (CB) of AgBr enhance the interfacial charge transfer that considered to reduce the probability of recombination of photo generated electrons and holes, that favor the illuminated photocatalytic activity of Ag-AgBr/HHST, meanwhile ensure the high stability of the composite[38].

4.1.1. Photo generated radical species for the degradation of OCs

To comprehend the role of active species concerned in the photo degradation of organic compounds. The (EPR) spin trapping-technique with (DMPO) was employed to detect and characterized the nature of active oxygen species generated on the surface of Ag-AgBr/HHST catalyst under visible and UV light irradiations. Four characteristic peaks of DMPO-·OH undoubtedly observed on the surface of Ag-AgBr/HHST in aqueous dispersion with intensity 1:2:2:1 in ESR signals, whereas no signal was observed in dark concluded that irradiation are essential for the generation of ·OH on the surface of the catalyst. Similarly six characteristic peaks of the DMPO$-O_2\cdot^-$ species detected on the surface of Ag-AgBr/HHST in methanolic dispersion, because the $O_2\cdot^-$ radicals are unstable in water and go through facile disproportionation reaction rather than slow reaction with DMPO (Fig. 14).

The formation of ·OH and $O_2\cdot^-$ radicals on the surface of illuminated Ag-AgBr/HHST provide a testimonial confirmation that the photocatalyst can efficiently excited under visible as well as UV light, to create electron-hole pairs and the charge separation maintained long enough to react with adsorbed oxygen to create a series of various oxidative species that finally decompose organic compounds. At the same time it can be noticeably seen that the intensity of hydroxyl radicals (·OH) and superoxide radicals ($O_2\cdot^-$) over Ag-AgBr/HHST under the UV light irradiation is superior than that of visible light, this account higher degradation capability toward aniline under UV light as compared to visible light.

5. Conclusions

A novel hollow hierarchical heterostructure photocatalyst synthesized by one-pot micro emulsification approach at optimum calcinations temperature (550 °C). The consequence outcomes of the cooperative characterizations exposed that sample possesses a hollow hierarchical spherical structures, consist of small-hollow-spheres@big-hollow-spheres, leading to the homogeneous distribution of the Ag and AgBr nano particles with an average particle size of 2–8 nm on the surface of the silica-titania matrix to figure heterostructure. Owing to the distinctive morphology, eminent surface area, tiny particles size and porous structure, the Ag-AgBr/HHST exhibited outstanding photocatalytic potential for the degradation of methyl orange and aniline under ultra violet as well as visible light irradiations in very short time intervals. The high photocatalytic performance can be attributed to the synergetic coupling of Ag and AgBr with silica-titania and due to exceptional hollow hierarchical morphology that facilitate the proficient transportation and separation of the photo generated charges during reaction hence boost up the photocatalytic performance.

Acknowledgments

This work was financially supported by the National Natural Science of Foundation of China (No. 21271017) and the national science and technology supporting plan of the twelth five-year (No. 2014BAE12B0101).

Appendix A. Supplementary data

Supplementary data associated with this article can be found, in the online version, at https://doi.org/10.1016/j.apcatb.2018.01.037.

References

[1] G. Liu, L. Wang, H.G. Yang, H.-M. Cheng, G.Q.M. Lu, Titania-based photocatalysts-crystal growth, doping and heterostructuring, J. Mater. Chem. 20 (2010) 831–843.
[2] H. Tong, S. Ouyang, Y. Bi, N. Umezawa, M. Oshikiri, J. Ye, Nano-photocatalytic materials: possibilities and challenges, Adv. Mater. 24 (2012) 229–251.
[3] A. Kudo, Y. Miseki, Heterogeneous photocatalyst materials for water splitting, Chem. Soc. Rev. 38 (2009) 253–278.
[4] X. Chen, S.S. Mao, Titanium dioxide nanomaterials: synthesis, properties, modifications, and applications, Chem. Rev. 107 (2007) 2891–2959.
[5] A. Fujishima, K. Honda, Electrochemical photolysis of water at a semiconductor electrode, Nature 238 (1972) 37–38.
[6] H. Sun, Y. Bai, Y. Cheng, W. Jin, N. Xu, Preparation and characterization of visible-light-driven carbon-sulfur-codoped TiO_2 photocatalysts, Ind. Eng. Chem. Res. 45 (2006) 4971–4976.
[7] H. Kato, A. Kudo, Visible-light-response and photocatalytic activities of TiO_2 and $SrTiO_3$ photocatalysts Co doped with antimony and chromium, J. Phys. Chem. B 106 (2002) 5029–5034.
[8] A. Kudo, Y. Miseki, Heterogeneous photocatalyst materials for water splitting, Chem. Soc. Rev. 38 (2009) 253–278.
[9] H.G. Yang, C.H. Sun, S.Z. Qiao, J. Zou, G. Liu, S.C. Smith, H.M. Cheng, G.Q. Lu, Anatase TiO_2 single crystals with a large percentage of reactive facets, Nature 453 (2008) 638–641.
[10] X. Chen, S.S. Mao, Titanium dioxide nanomaterials: synthesis, properties, modifications, and applications, Chem. Rev. 107 (2007) 2891–2959.
[11] J. Zhou, Y. Cheng, J. Yu, Preparation and characterization of visible-light-driven plasmonic photocatalyst Ag/AgCl/TiO_2 nanocomposite thin films, J. Photochem. Photobiol. A: Chem. 223 (2011) 82–87.
[12] Y. Ma, M. Xing, J. Zhang, B. Tian, F. Chen, Synthesis of well ordered mesoporous Yb, N co-doped TiO_2 with superior visible photocatalytic activity, Microporous Mesoporous Mater. 156 (2012) 145–152.
[13] M. Zhang, T. An, X. Liu, X. Hu, G. Sheng, J. Fu, Preparation of a high-activity ZnO/TiO_2 photocatalyst via homogeneous hydrolysis method with low temperature crystallization, Mater. Lett. 64 (2010) 1883–1886.
[14] X.-Z. Bu, G.-K. Zhang, Y.-Y. Gao, Y.-Q. Yang, Preparation and photocatalytic properties of visible light responsive N-doped TiO_2/rectorite composites, Microporous Mesoporous Mater. 136 (2010) 132–137.
[15] D.G. Calatayud, M. Rodríguez, B. Gallego, D. Fernández-Hevia, T. Jardiel, Preparación deMaterialesFotocatalizadoresBasados en $Bi_4Ti_3O_{12}$ Dopados con Metales de Transición, Boletín de la Sociedad Española de Cerámica y Vidrio 51 (2012) 55–60.
[16] R. Fagan, D.E. McCormack, D.D. Dionysiou, S.C. Pillai, A review of solar and visible light active TiO_2 photocatalysis for treating bacteria, cyanotoxins and contaminants of emerging concern, Mater. Sci. Semicond. Process. 42 (2016) 2–14.
[17] Y. Horiuchi, H. Yamashita, Design of mesoporous silica thin films containing single-site photocatalysts and their applications to superhydrophilic materials, Appl. Catal. A: Gen. 400 (2011) 1–8.
[18] C. Tan, G. Zhu, M. Hojamberdiev, C. Xu, J. Liang, P. Luo, Y. Liu, Room temperature synthesis and photocatalytic activity of magnetically recoverable Fe_3O_4/BiOCl nanocomposite photocatalysts, J. Cluster Sci. 24 (2013) 1115–1126.
[19] J. Rosen, G.S. Hutchings, F. Jiao, Ordered mesoporous cobalt oxide as highly efficient oxygen evolution catalyst, J. Am. Chem. Soc. 135 (2013) 4516–4521.
[20] D. Wang, Y. Duan, Q. Luo, X. Li, J. An, L. Bao, L. Shi, Novel preparation method for a new visible light photocatalyst: mesoporous TiO_2 supported Ag/AgBr, J. Mater. Chem. 22 (2012) 4847–4854.
[21] J. Zhang, B. Li, C. Han, J. Liu, One-pot synthesis of foamed titania-silica composite and its photocatalytic performance, Mater. Lett. 129 (2014) 50–53.
[22] H. Wang, X. Lang, J. Gao, W. Liu, D. Wu, Y. Wu, L. Guo, J. Li, Polyhedral AgBr microcrystals with an increased percentage of exposed {111} facets as a highly efficient visible-light photocatalyst, Chem.- Eur. J. 18 (2012) 4620–4626.
[23] P. Wang, B. Huang, X. Qin, X. Zhang, Y. Dai, J. Wei, M.H. Whangbo, Ag@AgCl: a highly efficient and stable photocatalyst active under visible light, Angew. Chem. 47 (2008) 7931–7933.
[24] H. Wang, X. Lang, J. Gao, W. Liu, D. Wu, Y. Wu, L. Guo, J. Li, Polyhedral AgBr microcrystals with an increased percentage of exposed {111} facets as a highly efficient visible-light photocatalyst, Chem.- Eur. J. 18 (2012) 4620–4626.
[25] H. Liu, S. Liu, Z. Zhang, X. Dong, T. Liu, Hydrothermal etching fabrication of TiO_2@graphene hollow structures: mutually independent exposed {001} and {101} facets nanocrystals and its synergistic photocaltalytic effects, Sci. Rep. 6 (2016) 33839.
[26] K.-N.P. Kumar, K. Keizer, A.J. Burggraaf, Textural evolution and phase transformation in titania membranes, J. Mater. Chem. 3 (1993) 1141–1149.
[27] A. Esmaeili, M.H. Entezari, Sonosynthesis of an Ag/AgBr/graphene-oxide nanocomposite as a solar photocatalyst for efficient degradation of methyl orange, J. Colloid Interface Sci. 466 (2016) 227–237.
[28] Y. Sui, C. Su, X. Yang, J. Hu, X. Lin, Ag-AgBr nanoparticles loaded on TiO_2 nanofibers as an efficient heterostructured photocatalyst driven by visible light, J. Mol. Catal. A: Chem. 410 (2015) 226–234.
[29] Y.-F. Chen, C.-Y. Lee, M.-Y. Yeng, H.-T. Chiu, The effect of calcination temperature on the crystallinity of TiO_2 nanopowders, J. Cryst. Growth 247 (2003) 363–370.

[30] Y. Guan, S. Wang, X. Wang, C. Sun, Y. Huang, C. Liu, H. Zhao, In situ self-assembled synthesis of Ag-AgBr/Al-MCM-41 with excellent activities of adsorption-photocatalysis, Appl. Catal. B: Environ. 209 (2017) 329–338.
[31] S.A. Khan, S. Ali, M. Sohail, M.A. Morsy, Z.H. Yamani, Fabrication of TiO_2/Ag/Ag_2O nanoparticles to enhance the photocatalytic activity of degussa P25 titania, Aust. J. Chem. 69 (2016) 41–46.
[32] X.-J. Lin, A.-Z. Zhong, Y.-B. Sun, X. Zhang, W.-G. Song, R.-W. Lu, A.-M. Cao, L.-J. Wan, In situ encapsulation of Pd inside the MCM-41 channel, Chem. Commun. 51 (2015) 7482–7485.
[33] I.A. Shkrob, M.C. Sauer, Hole scavenging and photo-stimulated recombination of electron-hole pairs in aqueous TiO_2 nanoparticles, J. Phys. Chem. B 108 (2004) 12497–12511.
[34] C. Minero, G. Mariella, V. Maurino, D. Vione, E. Pelizzetti, Photocatalytic transformation of organic compounds in the presence of inorganic ions. 2. Competitive reactions of phenol and alcohols on a titanium dioxide-fluoride system†, Langmuir: ACS J. Surf. Colloids 16 (2000) 8964–8972.
[35] C.-Y. Chang, Y.-H. Hsieh, L.-L. Hsieh, K.-S. Yao, T.-C. Cheng, Establishment of activity indicator of TiO_2 photocatalytic reaction-hydroxyl radical trapping method, J. Hazard. Mater. 166 (2009) 897–903.
[36] L. Kuai, B. Geng, X. Chen, Y. Zhao, Y. Luo, Facile subsequently light-induced route to highly efficient and stable sunlight-driven Ag-AgBr plasmonic photocatalyst, Langmuir: ACS J. Surf. Colloids 26 (2010) 18723–18727.
[37] D. Wang, Y. Duan, Q. Luo, X. Li, L. Bao, Visible light photocatalytic activities of plasmonic Ag/AgBr particles synthesized by a double jet method, Desalination 270 (2011) 174–180.
[38] G. Tian, Y. Chen, H.-L. Bao, X. Meng, K. Pan, W. Zhou, C. Tian, J.-Q. Wang, H. Fu, Controlled synthesis of thorny anatase TiO_2 tubes for construction of Ag-AgBr/TiO_2 composites as highly efficient simulated solar-light photocatalyst, J. Mater. Chem. 22 (2012) 2081–2088.
[39] L. Shi, L. Liang, J. Ma, Y. Meng, S. Zhong, F. Wang, J. Sun, Highly efficient visible light-driven Ag/AgBr/ZnO composite photocatalyst for degrading rhodamine B, Ceram. Int. 40 (2014) 3495–3502.
[40] C. Su, L. Liu, M. Zhang, Y. Zhang, C. Shao, Fabrication of Ag/TiO_2 nanoheterostructures with visible light photocatalytic function via a solvothermal approach, CrystEngComm 14 (2012) 3989–3999.
[41] H.W. Chen, Y. Ku, Y.L. Kuo, Photodegradation of o-cresol with Ag deposited on TiO_2 under visible and UV light irradiation, Chem. Eng. Technol. 30 (2007) 1242–1247.
[42] Y. Wang, Synthesis of plasmonic Ag@AgBr nanowires as highly efficient sunlight photocatalyst, J. Mater. Sci.: Mater. Electron. 27 (2016) 10122–10127.
[43] J. Li, J. Xu, W.-L. Dai, K. Fan, Dependence of Ag deposition methods on the photocatalytic activity and surface state of TiO_2 with twistlike helix structure, J. Phys. Chem. C 113 (2009) 8343–8349.
[44] P. Wang, B. Huang, X. Qin, X. Zhang, Y. Dai, M.-H. Whangbo, Ag/AgBr/$WO_3{\cdot}H_2O$: visible-light photocatalyst for bacteria destruction, Inorg. Chem. 48 (2009) 10697–10702.
[45] T. Zhou, Y. Xu, H. Xu, H. Wang, Z. Da, S. Huang, H. Ji, H. Li, In situ oxidation synthesis of visible-light-driven plasmonic photocatalyst Ag/AgCl/g-C_3N_4 and its activity, Ceram. Int. 40 (2014) 9293–9301.
[46] M. Lan, G. Fan, L. Yang, F. Li, Significantly enhanced visible-light-induced photocatalytic performance of hybrid Zn-Cr layered double hydroxide/graphene nanocomposite and the mechanism study, Ind. Eng. Chem. Res. 53 (2014) 12943–12952.
[47] R. Dadigala, B.R. Gangapuram, R. Bandi, A. Dasari, V. Guttena, Synthesis and characterization of C-TiO_2/$FeTiO_3$ and CQD/C-TiO_2/$FeTiO_3$ photocatalysts with enhanced photocatalytic activities under sunlight irradiation, Acta Metall. Sin. (English Letters) 29 (2016) 17–27.
[48] J. Ângelo, P. Magalhães, L. Andrade, A. Mendes, Characterization of TiO_2-based semiconductors for photocatalysis by electrochemical impedance spectroscopy, Appl. Surf. Sci. 387 (2016) 183–189.
[49] J. Smithyman, Q.H. Do, C. Zeng, Z. Liang, Ultra-fast aqueous Li-ion redox energy storage from vanadium oxide-carbon nanotube yarn electrodes, J. Power Sources 277 (2015) 59–63.
[50] X. Xu, G. Zhou, X. Dong, J. Hu, Interface band engineering charge transfer for 3D MoS_2 photoanode to boost photoelectrochemical water splitting, ACS Sustain. Chem. Eng. 5 (2017) 3829–3836.
[51] Y. Zhang, Z.-R. Tang, X. Fu, Y.-J. Xu, Nanocomposite of Ag-AgBr-TiO_2 as a photoactive and durable catalyst for degradation of volatile organic compounds in the gas phase, Appl. Catal. B: Environ. 106 (2011) 445–452.
[52] G. Liu, J. Zhao, Photocatalytic degradation of dye sulforhodamine B: a comparative study of photocatalysis with photosensitization, New J. Chem. 24 (2000) 411–417.
[53] Y. Wang, L. Liu, L. Xu, X. Cao, X. Li, Y. Huang, C. Meng, Z. Wang, W. Zhu, Ag_2 O/TiO_2/V_2O_5 one-dimensional nanoheterostructures for superior solar light photocatalytic activity, Nanoscale 6 (2014) 6790–6797.
[54] M. Strauss, M. Pastorello, F.A. Sigoli, J.M.d.S.e. Silva, I.O. Mazali, Singular effect of crystallite size on the charge carrier generation and photocatalytic activity of nano-TiO_2, Appl. Surf. Sci. 319 (2014) 151–157.
[55] D.S. Kim, S.J. Han, S.Y. Kwak, Synthesis and photocatalytic activity of mesoporous TiO_2 with the surface area, crystallite size, and pore size, J. Colloid Interface Sci. 316 (2007) 85–91.
[56] B. Pare, B. Sarwan, S.B. Jonnalagadda, Photocatalytic mineralization study of malachite green on the surface of Mn-doped BiOCl activated by visible light under ambient condition, Appl. Surf. Sci. 258 (2011) 247–253.
[57] L. Zhang, K.-H. Wong, Z. Chen, C.Y. Jimmy, J. Zhao, C. Hu, C.-Y. Chan, P.-K. Wong, AgBr-Ag-Bi_2WO_6 nanojunction system: a novel and efficient photocatalyst with double visible-light active components, Appl. Catal. A: Gen. 363 (2009) 221–229.
[58] H. Tada, T. Mitsui, T. Kiyonaga, T. Akita, K. Tanaka, All-solid-state Z-scheme in CdS-Au-TiO_2 three-component nanojunction system, Nat. Mater. 5 (2006) 782–786.
[59] L. Kronik, Y. Shapira, Surface photovoltage phenomena: theory, experiment, and applications, Surf. Sci. Rep. 37 (1999) 1–206.